Microscopic dynamics and viscoelasticity of vitrimers

Alessandro Perego, Daria Lazarenko, Michel Cloitre, Fardin Khabaz

Microscopic dynamics and viscoelasticity of vitrimers

Alessandro Perego[1], Daria Lazarenko[1], Michel Cloitre[2], and Fardin Khabaz[1,3*]

[1] School of Polymer Science and Polymer Engineering, The University of Akron, Akron, Ohio, 44325, USA

[2]Molecular, Macromolecular Chemistry, and Materials, ESPCI Paris, CNRS, PSL Research University, 75005 Paris, France

[3]Department of Chemical, Biomolecular, and Corrosion Engineering, The University of Akron, Akron, Ohio, 44325, USA

[*]Corresponding author email: fkhabaz@uakron.edu

[*]Corresponding author phone: 3309725410

Abstract

We implement a hybrid Molecular Dynamics /Monte Carlo simulation to study the microscopic dynamics and the macroscopic rheology of vitrimers with a fast bond exchange rate. We show that the linear viscoelastic properties and mean square displacement of the vitrimers collapse onto master curves by applying the same shift factors that follow the William-Landel-Ferry equation at low temperatures and Arrhenius-like behavior at high temperatures. The linkage between the microscopic dynamics and the linear rheology of vitrimers is established using the generalized Stokes-Einstein relationship, which efficiently extends the timescale of simulations and predicts the viscoelasticity. The values of the shift factors are related to the characteristic decay time of the intermediate scattering function which is accessible in scattering experiments. The same results hold in the case of an all-atom model of an ionic liquid. Our methodology provides a microscopic basis for the time-superposition principle and predicts the macroscopic rheology of thermo-rheologically simple vitrimers.

Keywords: Covalent adaptable networks, Thermoset, Vitrimer, Time-temperature-superposition, Microscopic dynamics, Viscoelasticity

Graphical Abstract

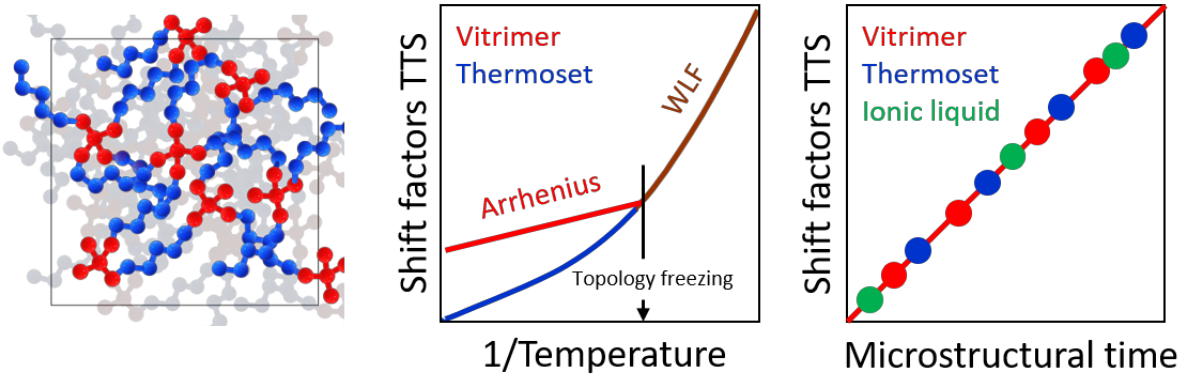

I. Introduction

Vitrimers are polymeric networks involving dynamic crosslinks which undergo reversible swap reactions at constant crosslink density, causing a change in their topology without loss of network integrity.[1] On heating, exchange reactions, which are thermally activated, become faster, allowing the network to rearrange its topology, relax stresses, and behave very much like a viscoelastic thermoplastic. On cooling, reactions slow down, and topological rearrangements become frozen, causing the vitrimer to behave like a thermoset. The thermoset-thermoplastic transition has been characterized by a topology freezing temperature, T_v, which is larger than the glass transition temperature T_g.[1, 2] These unique features make vitrimers interesting candidates for the design of amorphous and semicrystalline materials that combine dimensional stability at high temperatures, solvent resistance, ability to be reshaped and processed.[3-8] Following the pioneering work of Leibler and coworkers, who first synthesized vitrimers based on transesterification reactions,[1, 2] tremendous efforts have been made to design and implement various exchange reactions on a great variety of polymer backbones and architectures. Important developments of vitrimer chemistry, materials, and applications are discussed in recent reviews.[9-13]

A great challenge in applications is to develop vitrimers that relax mechanical stresses and exhibit small viscosity at relatively low temperatures. Small amplitude oscillatory shear measurements, stress relaxation, and creep are widespread methods for analyzing the macroscopic rheology of vitrimers. The stress relaxation times and the viscosity show an Arrhenius behavior reflecting thermal activation. Molecular dynamics simulations in conjunction with Mode-Coupling Theory have been used to explain this strong temperature dependence.[14] Besides temperature, relaxation in vitrimers has been shown to depend on many parameters: the presence and the nature of a catalyst,[2, 15] the bond exchange kinetics,[16-18] the structure[19-23] and the dynamics of the network,[24, 25] and the characteristics of the molecular

linkers used in linker-mediated vitrimers.[26, 27] Sciortino and coworkers introduced models to account for the dependence of the viscosity on the bond exchange time scale and showed that topological defects accelerate relaxation.[28, 29] Time-temperature superposition has been used to empirically extend the frequency window of observation in so-called thermo-rheologically simple vitrimers,[25, 30, 31] but it fails for vitrimers with many relaxation processes involving several temperatures dependences.[24, 26] Clearly a predictive understanding of the molecular mechanisms that control the macroscopic rheology of vitrimers is highly desirable. In this context, it appears crucial to go a step forward beyond macroscopic rheology by relating the microscopic molecular dynamics of vitrimers to their linear viscoelastic properties.

In this paper, we address this question by capitalizing on the coarse-grained molecular dynamics/Monte Carlo simulation we developed earlier.[32] We address the situation where the bond exchange is faster than the network dynamics. We compare the behavior of a permanently bonded thermoset and a vitrimer with bond exchanges, computing the storage and loss moduli, $G'(\omega)$ and $G''(\omega)$, the mean square displacements $\left\langle \Delta r^2(t) \right\rangle$ of the exchangeable monomeric units, the self-part of the van Hove function $G_s(r,t)$, and the intermediate scattering function $F_s(\mathbf{k},t)$. The microscopic dynamics of the exchangeable bonds are analogous to the cage dynamics of colloids. We demonstrate that time superposition indistinctly applies to $G'(\omega)$, $G''(\omega)$, and $\left\langle \Delta r^2(t) \right\rangle$ with the same shift factors that are simply related to the microscopic decay time of $F_s(\mathbf{k},t)$, which represents the microstructural relaxation time. Applying the generalized Stokes-Einstein relationship, we consistently recover the viscoelastic properties obtained by mechanically deforming the networks at small deformation from the microscopic dynamics. This demonstrates that the local motion of exchangeable groups at different temperatures controls the long-time relaxation of vitrimers. We discuss the relevance and the

validity of our results in relation to existing experiments. Preliminary results obtained for ionic liquids suggest that our results are general and may apply to other classes of soft materials.

II. Simulation details

A. Model description and method: A bead-spring model is first implemented to construct a three-dimensional network consisting of 1944 polymer chains with 5 monomeric units, called 5-mers, mixed with 972 tetra-functional crosslinkers (see Figure 1). This network mimics the microstructure of epoxy thermosets and vitrimers developed experimentally.[1] The non-bonded monomers interact through a shifted Lennard-Jones (LJ) potential. Bonded monomers interact through the finitely extensible nonlinear elastic (FENE) bond model.[33] The dimensionless distance ($\tilde{r}$), energy ($\tilde{U}$), and time ($\tilde{t}$) are determined by normalizing the distance (r), potential energy (U) which is the summation of the bonded and nonbonded interactions, and time (t) by the diameter of the monomers σ_{LJ}, the well-depth of the LJ potential ε_{LJ}, and $\sqrt{\sigma_{LJ}^2 m/\varepsilon_{LJ}}$ (m is the mass of the bead), respectively, in the simulations. The mixture of crosslinkers and 5-mers chains is initially relaxed in an NPT ensemble (at constant number of particles, pressure, and temperature) until the number density $\tilde{\rho}$ of the system reaches 0.844.[34] After this initial relaxation, the simulated annealing polymerization technique is used to efficiently connect the reacting beads of crosslinkers and 5-mers.[35, 36] The newly created bonds are then reduced in a stepwise fashion to an average FENE bond length of $0.96\sigma_{LJ}$ by applying a harmonic potential in a series of NVT ensembles. This final polymer network does not contain any loops or unreacted beads, and it is used as a reference to simulate the properties of a classic thermoset. During all simulations, a Nosé-Hoover thermostat and barostat are used to control temperature and pressure, respectively, with a time step $d\tilde{t} = 0.005$.

As the main feature of the vitrimer system is to have a constant number of exchangeable bonds at all temperatures, we use a discrete Monte Carlo (MC) step where at every 100 molecular dynamics (MD) step, the total energy cost of the bond exchange is determined as:

$$\Delta\tilde{U}_{Exchange} = \tilde{U}_{New}(i,l) + \tilde{U}_{New}(j,k) - \tilde{U}_{Old}(i,j) - \tilde{U}_{Old}(k,l), \quad (1)$$

where $\Delta\tilde{U}_{Exchange}$ is the change in the total energy of the system after the proposed move, and (i,j) and (k,l) are assumed to be two pairs of reactive beads connected by exchangeable bonds (see Fig. 1A) to different crosslinkers. This energy change involves recalculating the bonded (FENE) bond and non-bonded potentials (LJ). If $\Delta\tilde{U}_{Exchange} \le 0$, the proposed move is accepted right away, otherwise, the move is accepted with a probability based on the Metropolis acceptance criterion.[32, 37, 38]The detailed balance in the bond exchange reaction is respected by determining the MC move criteria based on the $\min\left\{1, \exp\left(-\Delta\tilde{U}_{Exchange}/k_BT\right)\right\}$ with k_B being the Boltzmann constant. According to the detailed balance principle, the flow of configurations between two states, *K*, is the same, i.e., $K(i \to j) = K(j \to i)$. This equality can be further expanded and rewritten as $n(i) \times Acc(i \to j) = n(j) \times Acc(j \to i)$, where $n(i)$ is the probability of the state *i* and $Acc(i \to j)$ represents the acceptance probability for the move $i \to j$. In the algorithm, we assume that the transition matrix for the Markov chain is symmetric; thus, the detailed balance equation reduces to the latter form (note that $n(i) \sim \exp\left(-\tilde{U}_i/k_BT\right)$). Considering the acceptance probability in our simulations, $\min\left\{1, \exp\left(-\Delta\tilde{U}_{Exchange}/k_BT\right)\right\}$, leads us to $\frac{Acc(i \to j)}{Acc(j \to i)} = \exp\left(-\frac{\Delta\tilde{U}_{Exchange}}{k_BT}\right)$ which indeed satisfies the detailed balance.[32, 37, 38]

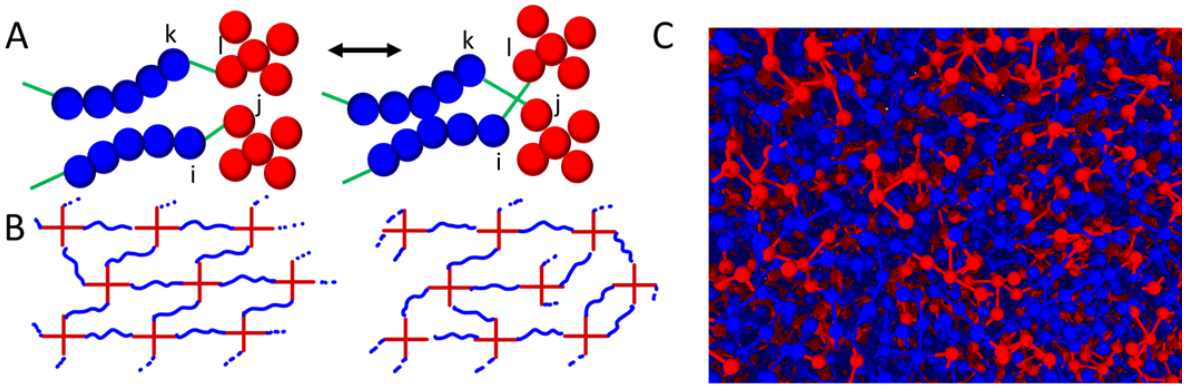

Figure 1. (A) Bond exchange reaction between the reactive units of the 5-mer chain (blue color) and tetra-functional crosslinkers (red color). (B) Mesoscopic view of the network at small scale before and after the bond swap. (C) Macroscopic view of the vitrimer network.

B. *Dynamic moduli calculation*. Small amplitude oscillatory shear (SAOS) simulations are performed using non-equilibrium molecular dynamics (NEMD)[39] by implementing the SLLOD equations of motion.[40, 41] The strain applied has the sinusoidal form of $\gamma(t) = \gamma_0 \sin(\tilde{\omega} t)$, where γ_0 is the strain amplitude and $\tilde{\omega}$ is the dimensionless frequency of the oscillatory shear deformation, $\tilde{\omega} = \omega\sqrt{\sigma_{LJ}^2 m/\varepsilon_{LJ}}$. The value of the strain amplitude γ_0 is set to 3% to ensure a linear viscoelastic regime.[32] The stress response of the system is computed by averaging the stress data obtained in 40-150 cycles of oscillations depending on the applied frequency, and fitting the average to $\tilde{\sigma}(t) = \tilde{\sigma}_0 \sin(\tilde{\omega} t + \delta)$, where $\tilde{\sigma}_0 = \sigma_0 \sigma_{LJ}^3/\varepsilon_{LJ}$ is the non-dimensional stress amplitude and δ is the phase angle. For that, we implement a fitting procedure based on the Trust Region Reflective (TRF) algorithm, where initial guesses are provided together with bounds. The maximum number of iterations for converging the fit is set to 1000. In practice, all the data are well-fitted to the sinusoidal stress response below this limit. The stress response is also checked using Fourier transform to ensure that there are no higher order harmonics. Results have been averaged over three independent replicas. Using these parameters, the dimensionless elastic $\tilde{G}'(\tilde{\omega})$ and viscous $\tilde{G}''(\tilde{\omega})$ moduli of the networks are determined using:

$$\tilde{G}'(\tilde{\omega}) = \frac{\tilde{\sigma}_0 \cos\delta}{\gamma_0} \tag{2}$$

$$\tilde{G}''(\tilde{\omega}) = \frac{\tilde{\sigma}_0 \sin\delta}{\gamma_0}. \tag{3}$$

III. Results and discussion:

III.A Transition temperatures: The networks are quenched from $\tilde{T} = k_B T / \varepsilon_{LJ} = 2.0$ to $\tilde{T} = 0.15$ in a stepwise fashion. The number density of polymer beads as a function of temperature is plotted in Figure 2A. Both the thermoset and the vitrimer network exhibit a glass transition at $\tilde{T}_g = 0.48 \pm 0.01$, determined from the intercept between the low and high temperature behaviors (see Figure 2A). We determine the variations with temperature of the coefficient of thermal expansion, $\tilde{\alpha} = \frac{1}{\tilde{V}}\left(\frac{\partial \tilde{V}}{\partial \tilde{T}}\right)_P$, from the density variations. As seen in Figure 2B, $\tilde{\alpha}$ reaches a maximum at a temperature slightly larger than the glass transition temperature $\tilde{T}_g$. At temperatures above the glass temperature, the thermal expansion coefficient of the thermoset, decreases and reaches a plateau. Due to bond exchange reactions, more free volume is available at the cross-linking points in the vitrimer network than in the thermoset, which leads to an increase in the specific volume. Consequently, the thermal expansion coefficient $\tilde{\alpha}$ of the vitrimer, first decreases, goes through a minimum and then increases. We associate the topology freezing temperature to the temperature where the initial decay of $\tilde{\alpha}$ and the subsequent increase intercept: $\tilde{T}_v = 0.65$. Above this temperature, the rate of bond exchange becomes comparable with the timescale of the simulations, and therefore the topology of the network changes more frequently; at the same time, the network integrity is preserved.

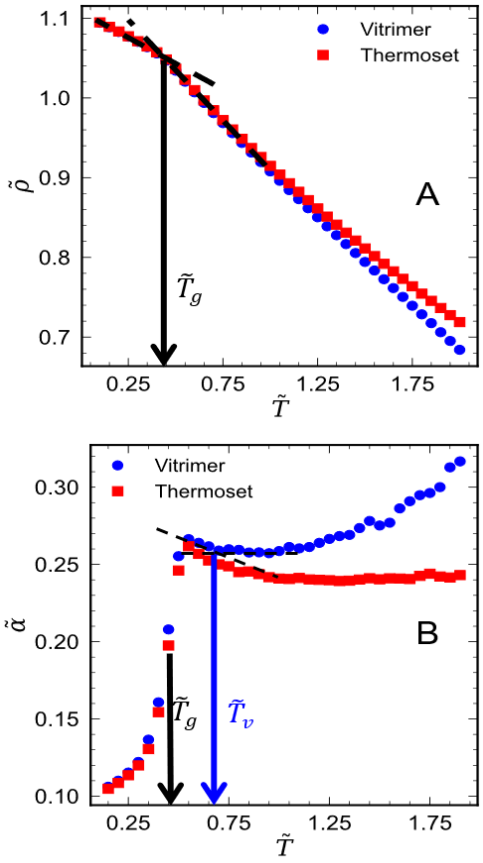

Figure 2. (A) Reduced number density $\tilde{\rho}$ ($\tilde{\rho} = N\sigma^3/V$, where V is the volume of the simulation box) and (B) thermal expansion coefficient $\tilde{\alpha}$ as a function of reduced temperature. Error bars are smaller than the symbol size.

III. B Linear viscoelasticity. We compute the elastic and viscous moduli of the networks versus frequency using small amplitude oscillatory shear simulations. Figure 3 shows the variations of the non-dimensional storage and loss moduli, $\tilde{G}' = G'\sigma_{LJ}^3/\varepsilon_{LJ}$ and $\tilde{G}'' = G''\sigma_{LJ}^3/\varepsilon_{LJ}$ where σ_{LJ} is the diameter of a monomer and ε_{LJ} is the energy well depth of the LJ potential, at different temperatures, for the thermoset and vitrimer networks. At low temperatures, the storage moduli of the thermoset and the vitrimer both go to a plateau value associated with glassy behavior. At high temperatures and in the low frequency regime, the storage modulus of the thermoset exhibits a plateau revealing rubbery behavior; by contrast the storage modulus of the vitrimer decreases suggesting the approach of terminal relaxation. While the storage moduli show a clear difference between the rheology of vitrimer and

thermoset, the loss moduli have similar variations. At low temperatures, the loss moduli increase with frequency, go through maxima and then decrease; at intermediate and high temperatures they decrease with decreasing frequency.

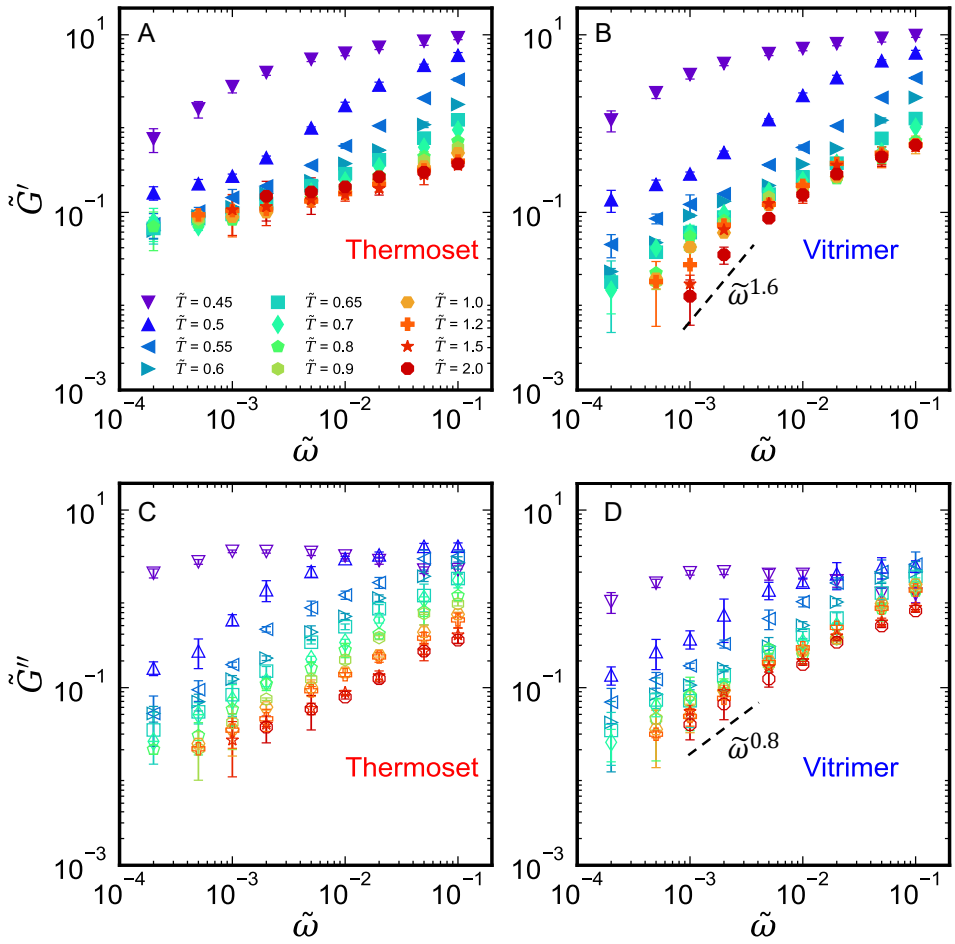

Figure 3. (A) and (B): storage moduli, $\tilde{G}'(\tilde{\omega})$, (C) and (D): loss moduli $\tilde{G}''(\tilde{\omega})$ of the model thermoset and vitrimer as a function of reduced frequency $\tilde{\omega} = \omega\sqrt{\sigma_{LJ}^2 m/\varepsilon_{LJ}}$ at different temperatures.

To rationalize the dependence of the viscoelastic moduli on temperature, we use time-temperature superposition (TTS). Van Gurp-Palmen plots of the phase angle δ ($\tan\delta = \tilde{G}''/\tilde{G}'$) versus the complex modulus $\tilde{G}^*$, as shown in Figures 4A-B for the thermoset and vitrimer, respectively, provide a good collapse of the data computed above the glass transition onto a unique master curve, supporting the validity of TTS for both the thermoset and the vitrimer.

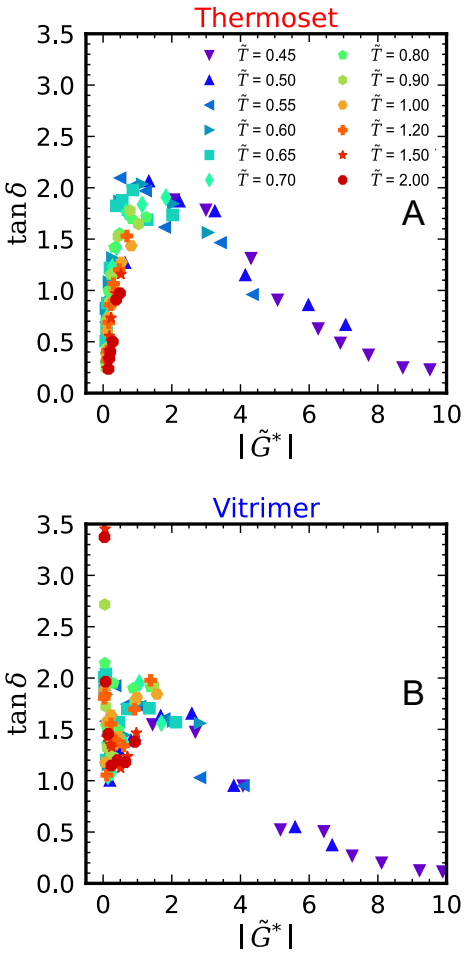

Figure. 4. van Gurp-Palmen plots of phase angle δ versus the magnitude of the complex $|G^*|$ modulus for the (A) thermoset and (B) vitrimer networks. Above the glass transition, the sets of data computed at different temperatures collapse on a master curve.

We set a reference temperature $\tilde{T}_0 = 0.6$, and starting from the high-frequency domain, we shift the storage and loss moduli data computed at different temperatures with respect to their value at the reference temperature in order to obtain continuous curves in log-log scale representation. The moduli are multiplied by a factor $b_T = \tilde{T}_0\tilde{\rho}_0 / \tilde{T}\tilde{\rho}$ where $\tilde{\rho}$ and $\tilde{\rho}_0$ are the number densities at $\tilde{T}$ and $\tilde{T}_0$, respectively, which can be computed from the volumetric properties. $b_T\tilde{G}'$ and $b_T\tilde{G}''$ are shifted along the frequency axis by the same shift factors a_T which will be analyzed below. Figure 5 shows the variations of $b_T\tilde{G}'(\omega)$ and $b_T\tilde{G}''(\omega)$ for the thermoset and the vitrimer networks as a function of the rescaled frequency $a_T\tilde{\omega}$.

The viscoelastic properties of the thermoset and vitrimer networks at high frequencies are similar. The high frequency/low temperature range corresponds to the glass regime where $\tilde{G}'$ reaches a high plateau value and $\tilde{G}''$ decreases with the frequency after reaching a maximum. Below the glass regime, there is an intermediate frequency range where the moduli decrease as power laws. The exponent is close to 0.5 for the thermoset, which is reminiscent of Rouse relaxation, and larger than 0.5 for the vitrimer. However, the strands connecting the crosslinks may be too short to exhibit Rouse relaxation and it is more likely that the observed variations are fortuitous and simply reflect the transition between the high frequency and low frequency domains. Additional simulations using networks with longer strands would clarify this issue.

For the thermoset, which is irreversibly crosslinked, the intermediate frequency range is followed at lower frequencies by a rubbery plateau that extends down to the lowest accessible frequencies. For the vitrimer network, it is interrupted by the approach of terminal relaxation caused by exchange reactions. At the lowest accessible frequencies, the storage and loss moduli vary like $G'(\omega) \propto \omega^{1.6}$ and $G''(\omega) \propto \omega^{0.8}$, respectively. These variations are different from those expected for terminal relaxation where $G'(\omega) \propto \omega^{2}$ and $G''(\omega) \propto \omega^{1}$. Clear terminal relaxation is not observed which indicates that there exists a broad distribution of relaxation times in the vitrimer. Simulations at much lower frequencies would enable to fully capture the terminal relaxation regime.

The difference between the behavior of vitrimer and thermoset at low frequencies can be attributed to the bond exchange rate which is equal to the reciprocal of the bond lifetime. The bond lifetime $\tilde{\tau}_b$ can be determined from the decay of the bond autocorrelation function as described in our previous works (see also Figures S1 and S2 in **Supporting Information**).[32, 42] At frequencies larger than $\tilde{\tau}_b^{-1}$, the vitrimer behaves similarly to the thermoset given that

the exchange time is longer than the deformation timescale, while at lower frequencies, bond exchange control the viscoelastic properties of the vitrimer.

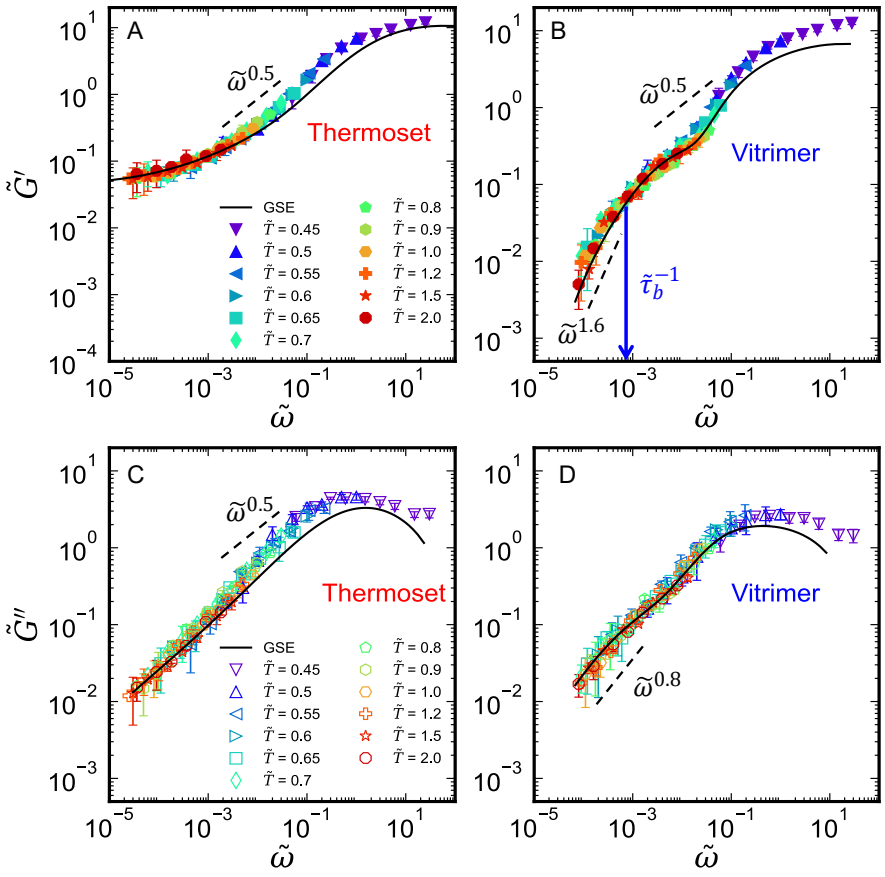

Figure 5. Master curves of rescaled storage ($b_T\tilde{G}'$) and loss ($b_T\tilde{G}''$) moduli, as a function of the reduced frequency $a_T\tilde{\omega}$ in the model thermoset (A and C) and vitrimer (B and D). The generalized Stokes-Einstein predictions are shown with continuous lines. The reference temperature is $\tilde{T}_0 = 0.6$. The blue arrow in B indicates the frequency corresponding to the average bond lifetime determined from the decay of the bond autocorrelation at the reference temperature (see Figures S1 and S2 in **Supporting Information**).

III. C Local displacements. We compute the mean square displacement (MSD), $\left\langle \Delta\tilde{r}^2 \right\rangle$, of the reactive beads that participate in the bond exchange reaction (*i.e.*, *i*, *j*, *k*, and *l* beads in Figure 1A) at different temperatures for both the thermoset and the vitrimer, as a function of time, as seen in Figure 6. We scale the MSD values with respect to the square of the particle diameter, σ_{LJ}^2. The thermoset network shows limited motion at all temperatures due to permanent crosslinking. At low temperatures, the MSDs of the vitrimer and thermoset are similar, while

at high temperatures the vitrimer network shows a nearly diffusive behavior. Given that the raw MSD curves seem to be superimposable by translation along the time scale (in log representation), we aim to construct master curves of the MSD for these two networks. By shifting the MSD data by factors a'_T along the horizontal axis in log scale representation with respect to the reference curve computed for $\tilde{T}_0 = 0.6$, we construct the master curves which are shown in Figures 6C and 6D. At very short times, both the thermoset and vitrimer networks are frozen in a glassy state and their MSDs exhibit a constant plateau that corresponds to the thermal vibration of the monomers with an amplitude of the order of $0.1\sigma_{LJ}$. As time increases, the mobility is enhanced in both networks due to thermal motion and it becomes subdiffusive with $\left\langle \Delta\tilde{r}^2 \right\rangle \sim \tilde{t}^{0.5}$; this regime corresponds to the intermediate frequency range in the viscoelastic spectra depicted in Figure 5. In the permanently crosslinked thermoset, the MSD values reach a constant plateau at long times showing that the displacements of monomers are spatially restricted. By contrast, when the vitrimer readjusts its topology upon heating, causing higher mobility of the reactive monomers, it shows a nearly diffusive behavior with $\left\langle \Delta\tilde{r}^2 \right\rangle \sim \tilde{t}$. In analogy with the caged dynamics of dense colloids,[43] each monomer can be viewed as embedded in a cage formed by the other units connected with the crosslinkers. The cage size is given by the maximum exploration of the monomers at long times, which is about two to three times their diameter. In thermosets, the cage lifetime is infinite, and the network segments only show cage-rattling motion. In vitrimers, bond exchange occurs as the temperature rises so that cages open and reactive monomers can escape and travel over long distances.

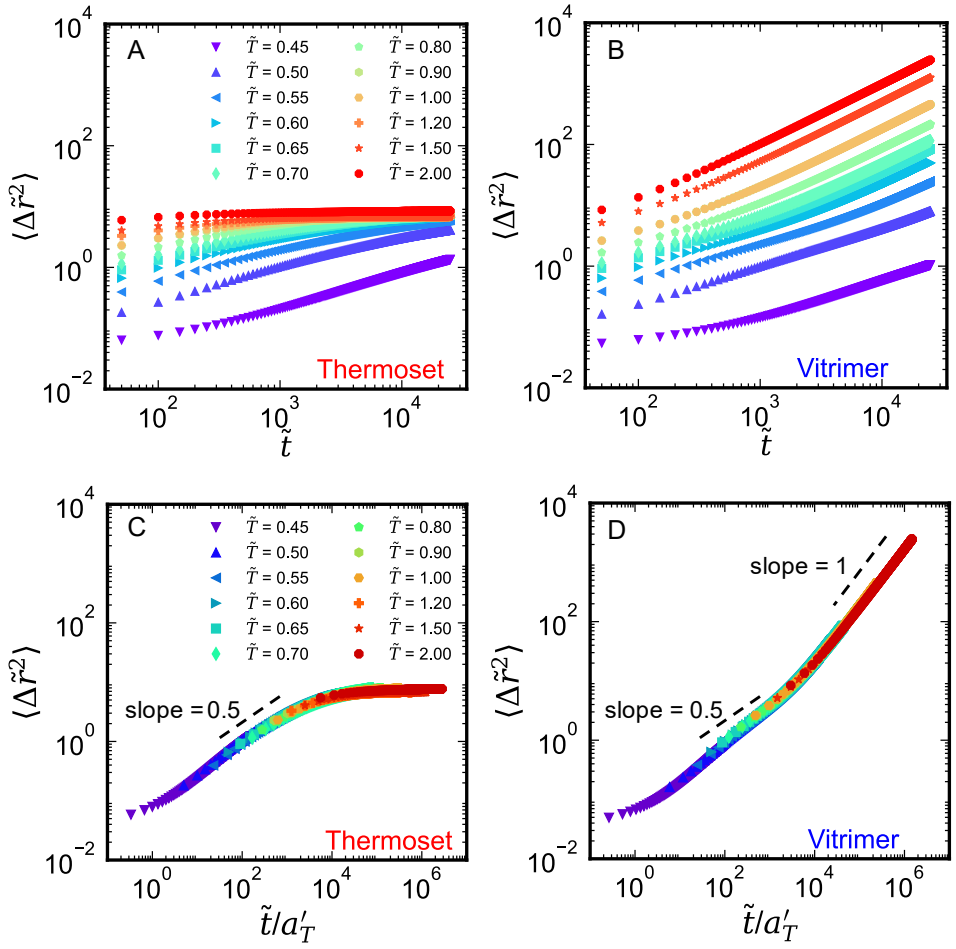

Figure 6. Mean squared displacement (MSD) $\left\langle \Delta\tilde{r}^2(\tilde{t}) \right\rangle$ of the reactive monomeric units that can participate in exchange reactions in thermoset (A) and vitrimer (B). Master curves of the MSD of (C) thermoset and (D) vitrimer. The reference temperature is $\tilde{T}_0 = 0.6$.

III.D Microscopic dynamics. To go further, we have calculated the self-part of the van Hove function, $G_S(\tilde{r},\tilde{t})$. The results computed for low and high temperatures, at short and long times, are plotted in Figure 7. In order to account for large differences in the displacements at low and high temperatures, we have rescaled the $\tilde{r}$ axis with the square root of the MSD at time $\tilde{t}$, i.e. $\sqrt{\left\langle \Delta\tilde{r}^2(\tilde{t}) \right\rangle}$. For comparison we also plot the Gaussian function $G_{s,Gauss.}(r) = \left(\frac{2}{\pi \left\langle \Delta r^2(t) \right\rangle} \right)^{3/2} \exp\left(-\frac{3r^2}{2\left\langle \Delta r^2(t) \right\rangle} \right)$. Figure 7 shows that the local dynamics are spatially heterogeneous at short and long times for both thermoset and vitrimer,[44, 45] but there are significant differences when the temperature is varied. At low temperature, below and

around $\tilde{T}_g$, the van Hove functions strongly deviate from the Gaussian function with an exponential tail which gives evidence for dynamical heterogeneities[44] in both the thermoset and the vitrimer. At high temperatures, above $\tilde{T}_g$, the variations of $G_S(\tilde{r},\tilde{t})$ confirm that monomers can move over large distances at long times in the vitrimer network but that they are confined in the thermoset. $G_S(\tilde{r},\tilde{t})$ becomes closer to the Gaussian form indicating that the motion is less affected by dynamical heterogeneities and becomes more homogeneous. It is interesting to note that some deviation persists although the MSD data show a nearly diffusive behavior at long time. Actually, diffusive behavior does not guarantee that the self-part of the van Hove functions are purely Gaussian, MSD data being average quantities over several modes of motion involving dynamical heterogeneities.[46-48]

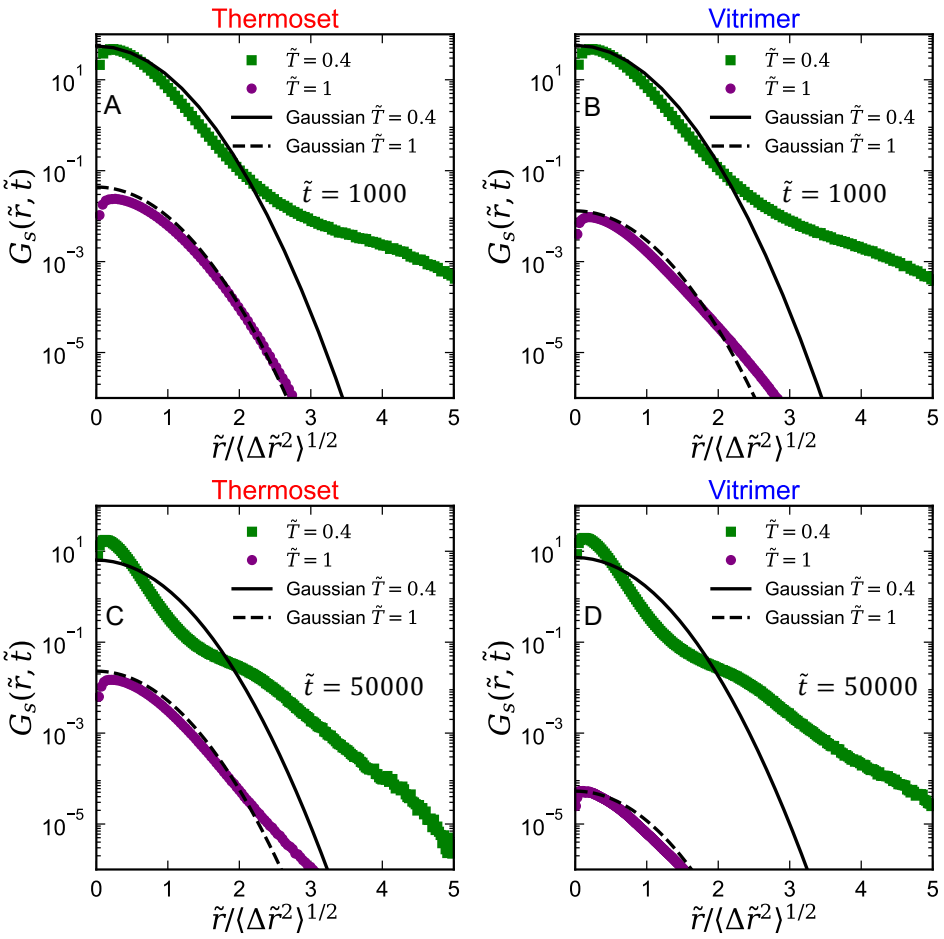

Figure 7. Self-part of the van Hove function for both the (A and C) thermoset and (B and D) vitrimer networks at short and long times at low and high temperatures as a function of rescaled distance by the square root of the MSD at time *t*.

III.E Microstructural relaxation. In order to characterize the cage dynamics of the monomers, we compute the incoherent intermediate scattering function (ISF) which describes the self- (or tagged particle) dynamics in Fourier space *via* the spatial wave vector (**k**)-dependent correlation function:[49] $F_s(\tilde{\mathbf{k}}, \tilde{t}) = \frac{1}{N}\left\langle \sum_{j=1}^{N} \exp\left[i\tilde{\mathbf{k}} \cdot \left(\tilde{\mathbf{r}}_j(\tilde{t}) - \tilde{\mathbf{r}}_j(0) \right) \right] \right\rangle$ where N is the total number of crosslinking monomers in the networks. The ISFs are computed at different temperatures at a wave vector amplitude $|\tilde{\mathbf{k}}| = 1.6$, which corresponds to the first peak at $\tilde{r} = 4$ of the radial distribution function of the crosslink center monomers. The dashed lines are the best fits of the ISFs to a stretched exponential function of the form of

$\frac{F_s(\tilde{\mathbf{k}},\tilde{t})-F_\infty}{1-F_\infty}=\exp\left(-\left(\frac{\tilde{t}}{\tilde{\tau}}\right)^{\beta}\right)$, where F_∞ is the value of the ISFs as $\tilde{t}\to\infty$, $\tilde{\tau}$ is the microstructural relaxation time, and β is the stretching exponent. The characteristic time is then determined from $\tilde{\tau}_c=\int_0^\infty F_s(\tilde{\mathbf{k}},\tilde{t})d\tilde{t}=\frac{\tilde{\tau}}{\beta}\Gamma\left(\frac{1}{\beta}\right)$, where Γ is the Gamma function. For each temperature, the ISF is well represented by this stretched exponential function giving access to a characteristic time $\tilde{\tau}_C$ which represents the microscopic time needed by a reacting monomer to escape from its cage. Figures 8C-D show that the ISFs of the thermoset and the vitrimer at different temperatures perfectly collapse onto master curves when they are plotted as a function of the reduced time $\tilde{t}/\tilde{\tau}_C$. At low temperatures ($\tilde{T}<\tilde{T}_g$), the master curves exhibit a plateau at short times, reflecting the in-cage motion of the monomers. At high temperatures, the ISFs of the thermoset reach a constant plateau at long times, whereas the ISFs of the vitrimer tend to zero since exchange reactions occur allowing cage rearrangements with a characteristic time $\tilde{\tau}_C$ and long-distance motions.

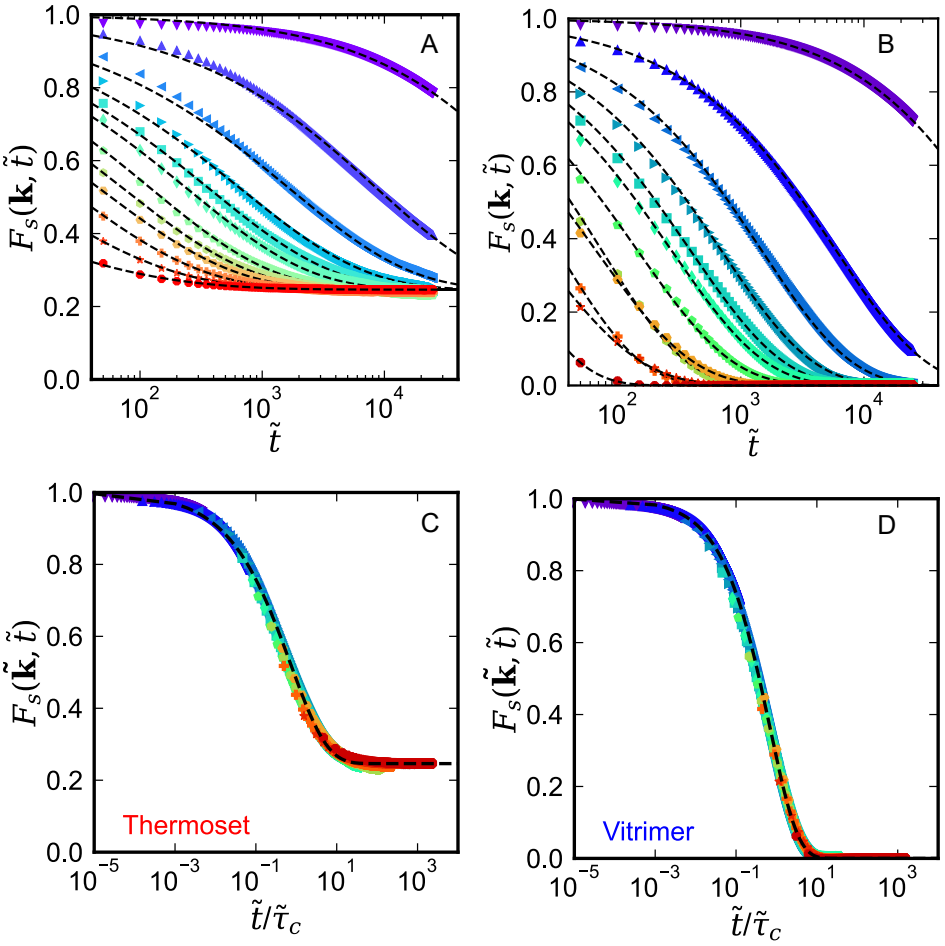

Figure 8. Intermediate scattering functions (ISF) of the reactive monomeric units that can participate in exchange reactions in thermoset (A) and vitrimer (C). Master curves of the ISF of (C) thermoset and (D) vitrimer as a function of the reduced time $\tilde{t}/\tilde{\tau}_C$. The color-coding is the same as the one used in Figure 6.

IV. Discussion. TTS indistinctly applies to the macroscopic viscoelastic properties, the mean square displacements of the reacting monomers and the intermediate scattering functions. The shift factors a_T and a'_T used to collapse the viscoelastic moduli and the MSD data computed at different temperatures are plotted together in Figure 9A as a function of $1/\tilde{T}$. At each temperature, we find that a_T and a'_T are comparable, showing that macroscopic rheology is intimately connected to the microscopic dynamics. The horizontal shift factors for the thermoset follow the Williams-Landel-Ferry's (WLF) equation for glassy polymers over the whole range of temperatures:[50] $\log(a_T) = \frac{-\tilde{C}_1(\tilde{T}-\tilde{T}_0)}{\tilde{C}_2+(\tilde{T}-\tilde{T}_0)}$, where $\tilde{T}_0$ is the reference temperature,

$\tilde{C}_1 = 2.26$ and $\tilde{C}_2 = 0.34$ are two fitting parameters ($\tilde{C}_1$ is a constant and $\tilde{C}_2$ is a dimensionless temperature). At low temperatures, the horizontal shift factors of the vitrimer follow the same WLF variation as the thermoset. At high temperatures, they can be well fitted to the Arrhenius equation: $\ln a_T = \frac{\tilde{A}}{\tilde{T}} + \tilde{C}$ with $\tilde{A} = 0.84$. The topology freezing temperature $\tilde{T}_v$ was defined by Leibler and coworkers as the value where the bond exchange dynamics between the network is slow enough to freeze the topology rearrangements in the network.[1] In agreement with our previously published work,[32, 42] we define $\tilde{T}_v$ as the temperature at which the horizontal shift factors a_T change from WLF to Arrhenius behavior: $\tilde{T}_v = 0.65$ (Figure 9A). This type of behavior has been observed experimentally for a variety of vitrimers.[24, 25, 27, 30, 31] We note that at the same temperature, the coefficient of thermal expansion shows a local minimum (Figure 2B). This value of $\tilde{T}_v$ is 1.5 times the glass transition temperature of the network ($\tilde{T}_g = 0.48$ This value also matches with our prior observations based on the temperature dependence of the probability of the bond exchange[42] and bond lifetime (see Fig. S2 in **Supporting Information**).

The temperature dependence of the microscopic relaxation time τ_C, which is plotted in Figure 9B, also shows WLF behavior for the thermoset and a combination of WLF and Arrhenius-like behaviors for the vitrimer. In view of the similarity of behavior exhibited by a_T, a_T', and τ_C, the shift factors must be related to the microscopic relaxation times through a relation of the form: $a_T = a_T' = \tau_C(T) / \tau_C(T_0)$. This is demonstrated in Figure 9C where the shift factors follow a linear relationship as a function of the reduced relaxation time $\tau_r = \tau_C(T) / \tau_C(T_0)$ over four decades.

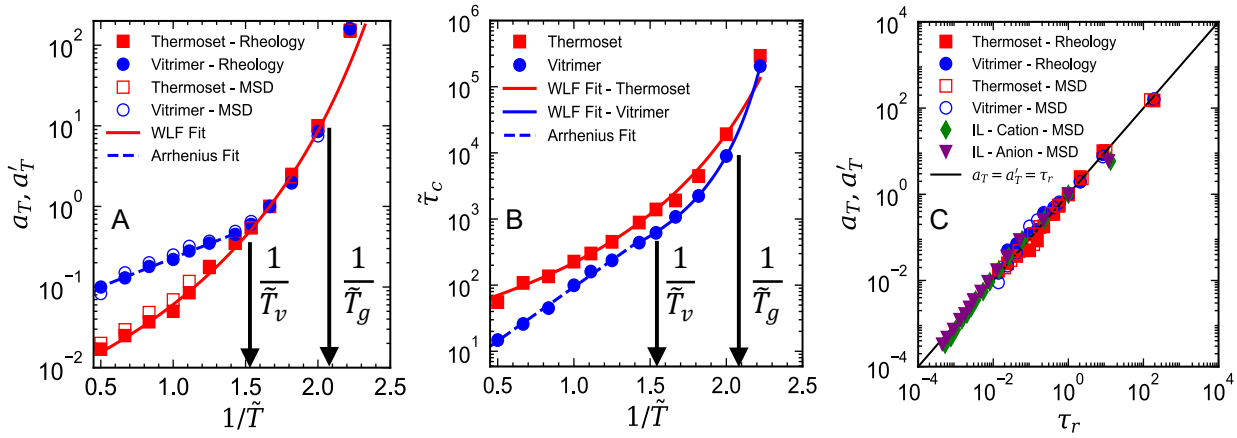

Figure 9. (A) Values of the horizontal shift factors used in collapsing the moduli and mean squared displacements for the thermoset and vitrimer. (B) Decay time ($\tilde{\tau}_c$) of the ISFs as a function of $1/\tilde{T}$. (C) Shift factors a_T (rheology) and a'_T (MSD) as a function of the reduced relaxation time, $\tau_r = \tilde{\tau}_c(T)/\tilde{\tau}_c(T_0)$ for thermoset, vitrimer, and ionic liquid systems. The continuous line represents a linear fitting to the data.

The successful application of identical shift factors to the viscoelastic moduli and the MSD suggests there is a quantitative relation between the microscopic dynamics and rheology of the network. This connection can be made using the generalized Stokes-Einstein equation (GSE), which relates the Laplace transform of the macroscopic modulus, $\tilde{G}(s)$, to the unilateral Laplace transform of the mean square displacements of Brownian tracers of radius R embedded in a viscoelastic matrix, $\left\langle \Delta\tilde{r}^2(s) \right\rangle$: $\tilde{G}(s) = \dfrac{k_B T}{\pi R s \left\langle \Delta\tilde{r}^2(s) \right\rangle}$.[52, 53] Here we consider that the tracers are the reactive units ($R = 0.5\sigma_{LJ}$). A direct numerical transform of the time-domain data to the frequency domain is generally unreliable and different methods to convert real time data to frequency data have been proposed.[52, 54] Here we implement the so-called Fourier microrheology method developed by Mason.[55] This method is approximate and subject to approximations that are detailed in **Supporting Information** SI1). As seen in Figures 4A-D, the agreement between the direct simulation moduli data and the prediction of the GSE relationship is satisfactory for the elastic and viscous moduli in both the thermoset and vitrimer networks, especially at intermediate and low frequencies. There is a slight discrepancy between

the data obtained from mechanical deformation and the GSE prediction at high frequencies, which we attribute to the breakdown of the GSE in the glassy state.[56] It is interesting to note that these microrheology data are obtained directly from the mobility of the reactive units, which are of monomeric size, without using any added large bead probing an effective medium. Failure of the GSE to yield macroscopic moduli has been reported in polymer solutions and melts when the probe size is too small.[57, 58] The success of the GSE equation here may be due to the fact that, although covalent bonds can exchange, there are no large scale topological defects in the networks so that the local environment of the monomers is representative of the bulk material. We do not claim however that the GSE must be working over the whole range of frequency and temperature for any network especially those exhibiting large scale defects. Fundamentally, treating the surrounding medium as a continuum is a useful idea for our systems, since the application of GSE can give us a picture of the viscoelastic properties of the material from data in the quiescent state, without performing time-consuming mechanical tests.

Figure 9C shows that it is possible to derive the TTS shift factors of the viscoelastic moduli and local displacements from the characteristic decay time of the intermediate scattering function. In order to evaluate the generality of this result, we have revisited atomistically-detailed MD simulations for an imidazolium-based ionic liquid.[59] This ionic liquid consists of the 1-(cyclohexylmethyl)-3-methylimidazolium cation ($[CyhmC_1im]^+$) and the bistriflimide anion ($[NTf_2]^-$). The detailed chemical structure and a description of the simulation procedure are given in **Supporting Information** (Figure S3 and SI2). We have previously reported that the simulated volumetric and linear viscoelastic properties of this ionic liquid are a good agreement with experiments.[59] In Figure 9C, we observe that the shift factors obtained from the master MSD curves both for the cation ($[CyhmC_1im]^+$) and anion ($[NTf_2]^-$) at different temperatures are collapsed on the same line $a_T = a'_T = \tau_r$ when they are

plotted against the rescaled ISF decay time. Thus, for simple thermo-rheological fluids, the correlation relating the shift factors to the microscopic relaxation times appears to be generic.

V. Conclusions

The simulations reported here qualitatively reproduce the experimental behavior found in thermo-rheologically simple vitrimers.[25, 30, 31] The main result is that TTS indistinctly applies to the macroscopic viscoelastic properties, the MSD of the reacting monomers, and the ISF. Therefore, the characteristic times associated with segmental relaxation, the Rouse relaxation of the network strands and the terminal relaxation all have the same temperature dependence. These results point to the key role of the local monomer-monomer friction in determining the macroscopic and microscopic dynamical properties. In this current vitrimer model, the rate of the exchange reaction is fast, the network is free of defect and there is no energy barrier. Thus we anticipate that the activation energy is small, which can be checked by converting $\tilde{A}$ in SI units using $E_a = 2.3R\tilde{A}\varepsilon_{LJ} / k_B$ where R is the perfect gas constant. A tentative estimate of E_a can be made for polyethylene by taking the approximate value of $\varepsilon_{LJ} = 0.686$ kJ/mol for CH_2 groups:[51] $E_a \cong 1.3$ kJ/mol. This activation energy is much less than in experimental systems where values in the range of 30-100 kJ/mol are found.[1-4, 25] Although this estimate must be considered for scaling purposes and not for direct comparison, it shows that the inclusion of defects in the networks and energy barriers for bond exchange are needed. We refer to the dynamics at work in this class of vitrimer as diffusion-limited. In future extensions of our simulations, we will investigate the case of slow reactions resulting in chemically-limited exchange process. This is achieved by adding temperature-dependent activation energy that slows down the bond exchange. Our expectation is that the exchange time and the network dynamics will have distinct temperature dependences leading to a failure of TTS as already reported in experiments.[24] Finally, the validity of TTS in diffusion-driven vitrimers opens new possibilities to efficiently extend the limited timescale of simulations and accurately predict the linear and nonlinear rheology of vitrimers. On the experimental level, the linear relationship between the relaxation times obtained from rheology and ISF decorrelation times, which is accessible from scattering experiments,

offers a route to determining the relaxation time of polymeric systems and calls for more studies on other types of soft matter.

Supporting Information:

- Autocorrelation function of exchangeable bonds $C(\tilde{t})$ as a function of simulation time at different temperatures (Fig. S1)
- Average lifetime $\tilde{\tau}_b$ of bonds as a function of temperature (Fig. S2)
- Chemical structure of the ionic liquid 1-(cyclohexylmethyl)-3-methylimidazolium $[CyhmC_1im]^+$ (cation) and bistriflimide $[NTf_2]^-$ (anion) (Fig. S3)
- Determination of viscoelastic moduli from mean-square displacements (SI1).
- Description of ionic liquid simulation (SI2).

References

1. Montarnal, D.; Capelot, M.; Tournilhac, F.; Leibler, L. Silica-Like Malleable Materials from Permanent Organic Networks. Science 2011, 334 (6058), 965-968.
2. Capelot, M.; Unterlass, M. M.; Tournilhac, F.; Leibler, L. Catalytic Control of the Vitrimer Glass Transition. ACS Macro Lett. 2012, 1 (7), 789-792.
3. Denissen, W.; Rivero, G.; Nicolaÿ, R.; Leibler, L.; Winne, J. M.; Du Prez, F. E. Vinylogous Urethane Vitrimers. Adv. Funct. Mater. 2015, 25 (16), 2451-2457.
4. Röttger, M.; Domenech, T.; Van Der Weegen, R.; Breuillac, A.; Nicolaÿ, R.; Leibler, L. High-Performance Vitrimers from Commodity Thermoplastics through Dioxaborolane Metathesis. Science 2017, 356 (6333), 62-65.
5. Demongeot, A.; Groote, R.; Goossens, H.; Hoeks, T.; Tournilhac, F.; Leibler, L. Cross-Linking of Poly(Butylene Terephthalate) by Reactive Extrusion Using Zn(Ii) Epoxy-Vitrimer Chemistry. Macromolecules 2017, 50 (16), 6117-6127.
6. Kar, G. P.; Saed, M. O.; Terentjev, E. M. Scalable Upcycling of Thermoplastic Polyolefins into Vitrimers through Transesterification. J. Mater. Chem. A 2020, 8 (45), 24137-24147.
7. Wang, Z.; Gu, Y.; Ma, M.; Chen, M. Strong, Reconfigurable, and Recyclable Thermosets Cross-Linked by Polymer–Polymer Dynamic Interaction Based on Commodity Thermoplastics. Macromolecules 2020, 53 (3), 956-964.
8. Farge, L.; Hoppe, S.; Daujat, V.; Tournilhac, F.; André, S. Solid Rheological Properties of Pbt-Based Vitrimers. Macromolecules 2021, 54 (4), 1838-1849.
9. Kloxin, C. J.; Bowman, C. N. Covalent Adaptable Networks: Smart, Reconfigurable and Responsive Network Systems. Chem. Soc. Rev. 2013, 42 (17), 7161-7173.
10. Scheutz, G. M.; Lessard, J. J.; Sims, M. B.; Sumerlin, B. S. Adaptable Crosslinks in Polymeric Materials: Resolving the Intersection of Thermoplastics and Thermosets. J. Am. Chem. Soc. 2019, 141 (41), 16181-16196.
11. Winne, J. M.; Leibler, L.; Du Prez, F. E. Dynamic Covalent Chemistry in Polymer Networks: A Mechanistic Perspective. Polym. Chem. 2019, 10 (45), 6091-6108.
12. Guerre, M.; Taplan, C.; Winne, J. M.; Du Prez, F. E. Vitrimers: Directing Chemical Reactivity to Control Material Properties. Chem. Sci. 2020, 11 (19), 4855-4870.
13. Van Zee, N. J.; Nicolaÿ, R. Vitrimers: Permanently Crosslinked Polymers with Dynamic Network Topology. Prog. Polym. Sci. 2020, 104, 101233.
14. Lei, Q.-L.; Xia, X.; Yang, J.; Pica Ciamarra, M.; Ni, R. Entropy-Controlled Cross-Linking in Linker-Mediated Vitrimers. Proc. Natl. Acad. Sci. 2020, 117 (44), 27111-27115.
15. Self, J. L.; Dolinski, N. D.; Zayas, M. S.; Read de Alaniz, J.; Bates, C. M. Brønsted-Acid-Catalyzed Exchange in Polyester Dynamic Covalent Networks. ACS Macro Lett. 2018, 7 (7), 817-821.
16. Schoustra, S. K.; Dijksman, J. A.; Zuilhof, H.; Smulders, M. M. J. Molecular Control over Vitrimer-Like Mechanics – Tuneable Dynamic Motifs Based on the Hammett Equation in Polyimine Materials. Chem. Sci. 2021, 12 (1), 293-302.
17. Van Herck, N.; Maes, D.; Unal, K.; Guerre, M.; Winne, J. M.; Du Prez, F. E. Covalent Adaptable Networks with Tunable Exchange Rates Based on Reversible Thiol–Yne Cross-Linking. Angew. Chem. Int. Ed. 2020, 59 (9), 3609-3617.
18. El-Zaatari, B. M.; Ishibashi, J. S.; Kalow, J. A. Cross-Linker Control of Vitrimer Flow. Polym. Chem. 2020, 11 (33), 5339-5345.
19. Spiesschaert, Y.; Taplan, C.; Stricker, L.; Guerre, M.; Winne, J. M.; Du Prez, F. E. Influence of the Polymer Matrix on the Viscoelastic Behaviour of Vitrimers. Polym. Chem. 2020, 11 (33), 5377-5385.

20. Parada, G. A.; Zhao, X. Ideal Reversible Polymer Networks. Soft Matter 2018, 14 (25), 5186-5196.
21. Gablier, A.; Saed, M. O.; Terentjev, E. M. Rates of Transesterification in Epoxy–Thiol Vitrimers. Soft Matter 2020, 16 (22), 5195-5202.
22. Chen, M.; Si, H.; Zhang, H.; Zhou, L.; Wu, Y.; Song, L.; Kang, M.; Zhao, X.-L. The Crucial Role in Controlling the Dynamic Properties of Polyester-Based Epoxy Vitrimers: The Density of Exchangeable Ester Bonds (Y). Macromolecules 2021, 54 (21), 10110-10117.
23. Ricarte, R. G.; Tournilhac, F.; Cloître, M.; Leibler, L. Linear Viscoelasticity and Flow of Self-Assembled Vitrimers: The Case of a Polyethylene/Dioxaborolane System. Macromolecules 2020, 53 (5), 1852-1866.
24. Ricarte, R. G.; Shanbhag, S. Unentangled Vitrimer Melts: Interplay between Chain Relaxation and Cross-Link Exchange Controls Linear Rheology. Macromolecules 2021, 54 (7), 3304-3320.
25. Porath, L. E.; Evans, C. M. Importance of Broad Temperature Windows and Multiple Rheological Approaches for Probing Viscoelasticity and Entropic Elasticity in Vitrimers. Macromolecules 2021, 54 (10), 4782-4791.
26. Soman, B.; Evans, C. M. Effect of Precise Linker Length, Bond Density, and Broad Temperature Window on the Rheological Properties of Ethylene Vitrimers. Soft Matter 2021, 17 (13), 3569-3577.
27. Wu, S.; Yang, H.; Huang, S.; Chen, Q. Relationship between Reaction Kinetics and Chain Dynamics of Vitrimers Based on Dioxaborolane Metathesis. Macromolecules 2020, 53 (4), 1180-1190.
28. Smallenburg, F.; Leibler, L.; Sciortino, F. Patchy Particle Model for Vitrimers. Phys. Rev. Lett. 2013, 111 (18), 188002.
29. Ciarella, S.; Sciortino, F.; Ellenbroek, W. G. Dynamics of Vitrimers: Defects as a Highway to Stress Relaxation. Phys. Rev. Lett. 2018, 121 (5), 058003.
30. Snijkers, F.; Pasquino, R.; Maffezzoli, A. Curing and Viscoelasticity of Vitrimers. Soft Matter 2017, 13 (1), 258-268.
31. Fang, H.; Fang, H.; Fang, H.; Ye, W.; Ding, Y.; Ding, Y.; Winter, H. H. Rheology of the Critical Transition State of an Epoxy Vitrimer. Macromolecules 2020, 53 (12), 4855-4862.
32. Perego, A.; Khabaz, F. Volumetric and Rheological Properties of Vitrimers: A Hybrid Molecular Dynamics and Monte Carlo Simulation Study. Macromolecules 2020, 53 (19), 8406-8416.
33. Warner, H. R. Kinetic Theory and Rheology of Dilute Suspensions of Finitely Extendible Dumbbells. Ind. Eng. Chem. Fundam. 1972, 11 (3), 379-387.
34. Everaers, R.; Karimi-Varzaneh, H. A.; Fleck, F.; Hojdis, N.; Svaneborg, C. Kremer-Grest Models for Commodity Polymer Melts: Linking Theory, Experiment, and Simulation at the Kuhn Scale. Macromolecules 2020, 53 (6), 1901–1916.
35. Khabaz, F.; Mani, S.; Khare, R. Molecular Origins of Dynamic Coupling between Water and Hydrated Polyacrylate Gels. Macromolecules 2016, 49 (19), 7551-7562.
36. Khare, R.; Paulaitis, M. E.; Lustig, S. R. Generation of Glass Structures for Molecular Simulations of Polymers Containing Large Monomer Units: Application to Polystyrene. Macromolecules 1993, 26 (26), 7203-7209.
37. Wilson, M.; Rabinovitch, A.; Baljon, A. R. C. Computational Study of the Structure and Rheological Properties of Self-Associating Polymer Networks. Macromolecules 2015, 48 (17), 6313-6320.
38. Frenkel, D.; Smit, B., Understanding Molecular Simulation: From Algorithms to Applications. Academic Press: 1996.

39. Berker, A.; Chynoweth, S.; Klomp, U. C.; Michopoulos, Y. Non-Equilibrium Molecular Dynamics (Nemd) Simulations and the Rheological Properties of Liquid N-Hexadecane. J. Chem. Soc., Faraday Trans. 1992, 88 (13), 1719-1725.
40. Evans, D. J.; Morriss, G. P. Nonlinear-Response Theory for Steady Planar Couette Flow. Phys. Rev. A 1984, 30 (3), 1528-1530.
41. Daivis, P. J.; Todd, B. D. Direct Derivation and Proof of the Validity of the Sllod Equations of Motion for Generalized Homogeneous Flows. J. Chem. Phys. 2006, 124 (19), 194103.
42. Perego, A.; Khabaz, F. Effect of Bond Exchange Rate on Dynamics and Mechanics of Vitrimers. J. Polym. Sci. 2021, 59 (21), 2590-2602.
43. Pusey, P. N., Liquids, Freezing and Glass Transition. North Holland: 1991.
44. Kob, W.; Donati, C.; Plimpton, S. J.; Poole, P. H.; Glotzer, S. C. Dynamical Heterogeneities in a Supercooled Lennard-Jones Liquid. Phys. Rev. Lett. 1997, 79 (15), 2827-2830.
45. Angell, C. A.; Ngai, K. L.; Mckenna, G. B.; Mcmillan, P. F.; Martin, S. W. Relaxation in Glassforming Liquids and Amorphous Solids. J. Appl. Phys. 2000, 88 (6), 3113-3157.
46. Rusciano, F.; Pastore, R.; Greco, F. Fickian Non-Gaussian Diffusion in Glass-Forming Liquids. Phys. Rev. Lett. 2022, 128 (16), 168001.
47. Chechkin, A. V.; Seno, F.; Metzler, R.; Sokolov, I. M. Brownian yet Non-Gaussian Diffusion: From Superstatistics to Subordination of Diffusing Diffusivities. Phys. Rev. X 2017, 7 (2), 021002.
48. Uneyama, T.; Miyaguchi, T.; Akimoto, T. Fluctuation Analysis of Time-Averaged Mean-Square Displacement for the Langevin Equation with Time-Dependent and Fluctuating Diffusivity. Phys. Rev. E 2015, 92 (3), 032140.
49. Yamamoto, R.; Onuki, A. Heterogeneous Diffusion in Highly Supercooled Liquids. Phys. Rev. Lett. 1998, 81 (22), 4915-4918.
50. Ferry, J. D., Viscoelastic Properties of Polymers. 3 ed.; Wiley: 1980.
51. Pant, P. V. K.; Han, J.; Smith, G. D.; Boyd, R. H. A Molecular Dynamics Simulation of Polyethylene. J. Chem. Phys. 1993, 99 (1), 597-604.
52. Furst, E. M.; Squires, T. M., Microrheology. Oxford University Press: 2017.
53. Mason, T. G.; Weitz, D. A. Optical Measurements of Frequency-Dependent Linear Viscoelastic Moduli of Complex Fluids. Phys. Rev. Lett. 1995, 74 (7), 1250.
54. Li, Q.; Peng, X.; Chen, D.; McKenna, G. B. The Laplace Approach in Microrheology. Soft Matter 2020, 16 (14), 3378-3383.
55. Mason, T. G. Estimating the Viscoelastic Moduli of Complex Fluids Using the Generalized Stokes-Einstein Equation. Rheol. Acta 2000, 39 (4), 371-378.
56. Kumar, S. K.; Szamel, G.; Douglas, J. F. Nature of the Breakdown in the Stokes-Einstein Relationship in a Hard Sphere Fluid. J. Chem. Phys. 2006, 124 (21), 214501.
57. Ge, T.; Grest, G. S.; Rubinstein, M. Nanorheology of Entangled Polymer Melts. Phys. Rev. Lett. 2018, 120 (5), 057801.
58. Lu, Q.; Solomon, M. J. Probe Size Effects on the Microrheology of Associating Polymer Solutions. Phys. Rev. E 2002, 66 (6), 061504.
59. Balogun, A.; Lazarenko, D.; Khabaz, F.; Khare, R. Extending the Timescale of Molecular Simulations by Using Time–Temperature Superposition: Rheology of Ionic Liquids. Soft Matter 2021, 17 (30), 7210-7220.

Supporting Information: Microscopic dynamics and viscoelasticity of vitrimers

Alessandro Perego[1], Daria Lazarenko[1], Michel Cloitre[2], and Fardin Khabaz[1,3]

[1] School of Polymer Science and Polymer Engineering, The University of Akron, Akron, Ohio, 44325, USA

[2]Molecular, Macromolecular Chemistry, and Materials, ESPCI Paris, CNRS, PSL Research University, 75005 Paris, France

[3]Department of Chemical, Biomolecular, and Corrosion Engineering, The University of Akron, Akron, Ohio, 44325, USA

[*]Corresponding author email: fkhabaz@uakron.edu

Table of Contents

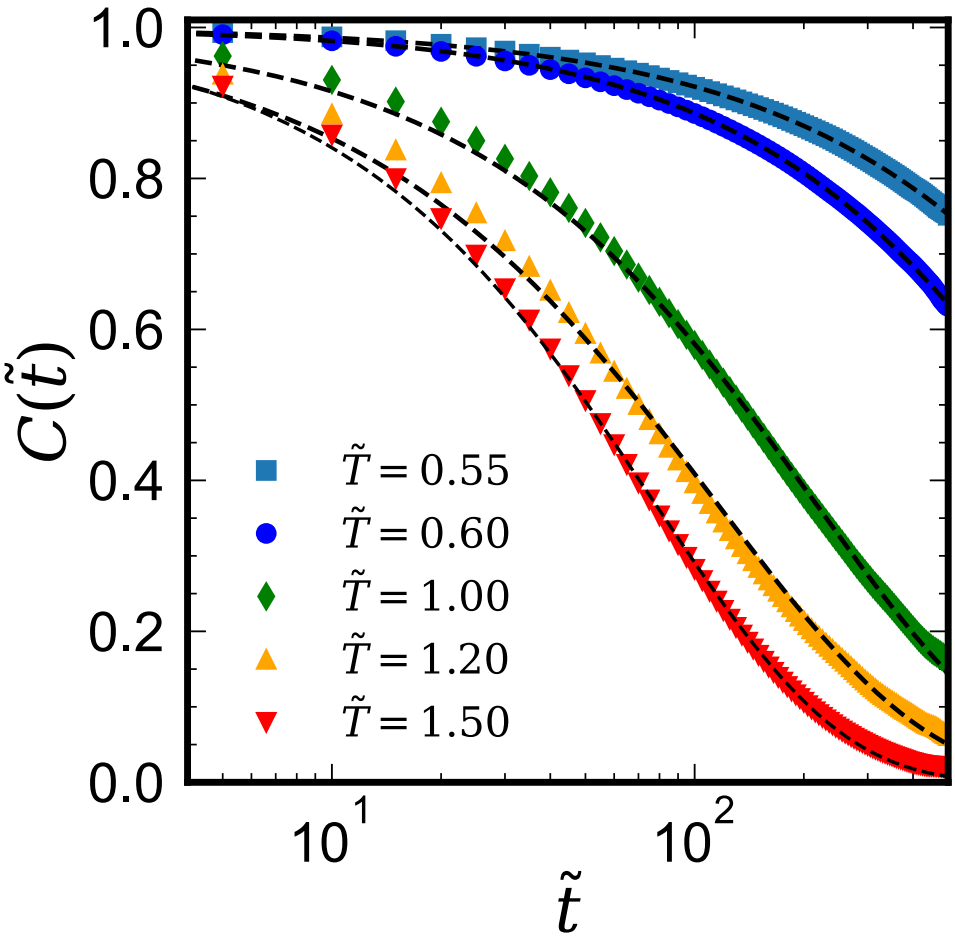

Figure S1: Autocorrelation function of exchangeable bonds, $C(\tilde{t})$, as a function of simulation time at different temperatures. The autocorrelation function is defined by $C(\tilde{t}) = \frac{\langle H(\tilde{t})H(0)\rangle}{\langle H(0)^2\rangle}$, where $H(\tilde{t})$ represents a binary function such as $H(\tilde{t}) = 1$ if two pairs of crosslinking beads are connected, and $H(\tilde{t}) = 0$ otherwise. At low temperature ($\tilde{T} \le \tilde{T}_g$), the bond exchange reaction is slow, and therefore the $C(\tilde{t})$ function does not decay significantly and shows a value close to unity. As the temperature increases, $C(\tilde{t})$ shows a stretched exponential decay with $C(\tilde{t})$ dropping faster at higher temperatures. Fits to stretched exponential functions are shown using dashed lines.

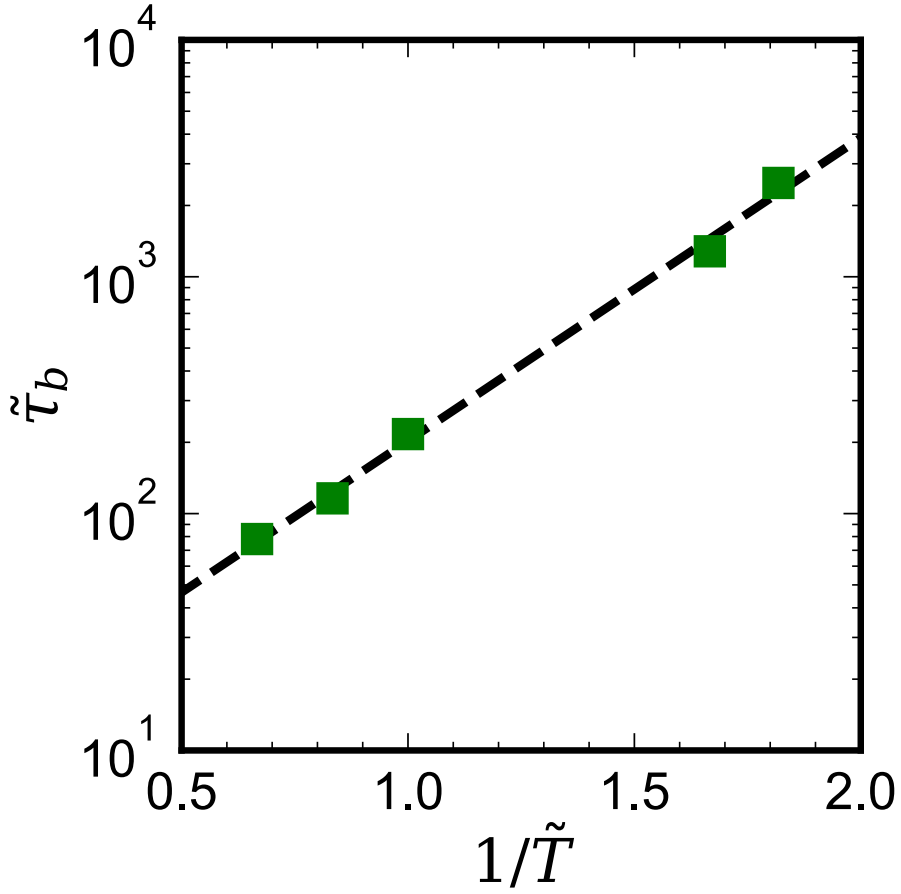

Figure S2: Average lifetime $\tilde{\tau}_b$ of bonds as a function of temperature. The dashed line shows the Arrhenius fit to the data, $\ln \tilde{\tau}_b = \frac{\tilde{A}'}{\tilde{T}} + \tilde{C}$. The values of $\tilde{\tau}_b$ are determined from the decay timescale of $C(\tilde{t})$ in Figure S2. The activation energy of the Arrhenius-like relaxation can be easily obtained from $\tilde{A}'$.

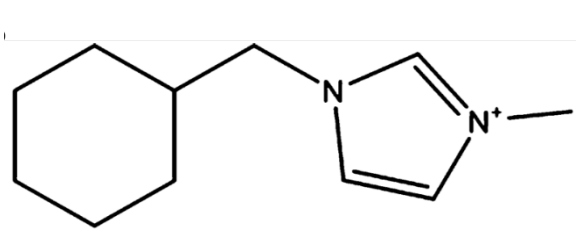

$[CyhmC_1im]^+$

(A)

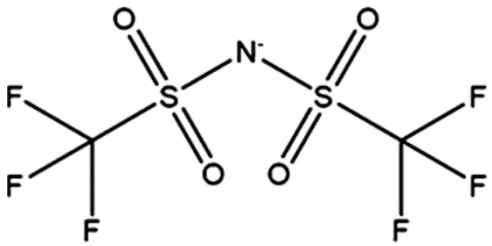

$[NTf_2]^-$

(B)

Figure S3: Chemical structure of the ionic liquid 1-(cyclohexylmethyl)-3-methylimidazolium $[CyhmC_1im]^+$ (cation) and bistriflimide $[NTf_2]^-$ (anion).

SI1: Determination of viscoelastic moduli from mean-square displacements

The generalized Stokes-Einstein equation (GSE) relates the Laplace transform of the macroscopic modulus, $\tilde{G}(s)$, to the unilateral Laplace transform of the mean square displacements of Brownian tracers of radius *R* embedded in a viscoelastic matrix:[1, 2]

$$\left\langle \Delta\tilde{r}^2(s)\right\rangle :\ \tilde{G}(s)=\frac{k_BT}{\pi Rs\left\langle \Delta\tilde{r}^2(s)\right\rangle} \tag{1}$$

A direct numerical transform of the time-domain data to the frequency domain is generally unreliable and different methods to convert real time data to frequency data have been proposed.[2,3] In this work we use the so-called Fourier microrheology method developed by Mason.[4] He demonstrated that a similar GSE exists in the Fourier domain:

$$G^*(\omega)=\frac{k_BT}{\pi Ri\omega\Im\left\langle \Delta r^2(t)\right\rangle} \tag{2}$$

where $\Im\left(\left\langle \Delta r^2\left(t\right)\right\rangle\right)$ is the Fourier transform of $\left\langle \Delta r^2\left(t\right)\right\rangle$. Expression (2) can also be obtained from (1) by using the analytical continuation $s=i\omega$.

To compute the complex modulus $G^*(\omega)$, the mean squared displacement $\left\langle \Delta r^2(t)\right\rangle$ is expanded at each sampled time $t_0=1/\omega$ by a power law function:

$$\left\langle \Delta r^2(t)\right\rangle \approx \left\langle \Delta r^2(1/\omega)\right\rangle (\omega t)^{\alpha(\omega)} \tag{3}$$

where $\alpha(\omega)$ is the logarithmic slope of the MSD at t_0:

$$\alpha(\omega)=\left.\frac{\mathrm{d}\ln\left(\left\langle \Delta r^2(t)\right\rangle\right)}{\mathrm{d}\,t}\right|_{t=1/\omega} \tag{4}$$

The Fourier transform of the power law (3) leads to the relation:

$$i\omega\Im\left[\left\langle \Delta r^2(t)\right\rangle\right]=\left\langle \Delta r^2(1/\omega)\right\rangle\Gamma\left[1+\alpha\left(\omega\right)\right]i^{-\alpha(\omega)} \tag{5}$$

It is assumed here that the values of $\left\langle \Delta r^2(t)\right\rangle$ at times very different from $1/\omega$ do not contribute significantly to the Fourier transform. Γ is the gamma function. Substituting and rearranging, we obtain:

$$\begin{aligned}\left|G^*(\omega)\right| &= \frac{k_BT}{\pi R\left\langle \Delta r^2(1/\omega)\right\rangle\Gamma\left[1+\alpha(\omega)\right]}\\ G'(\omega) &= \left|G^*(\omega)\right|\cos\left[\pi\alpha(\omega)\right]\\ G''(\omega) &= \left|G^*(\omega)\right|\sin\left[\pi\alpha(\omega)\right]\end{aligned} \tag{6}$$

SI2: Ionic liquid simulation

For intermolecular and intramolecular interactions, the general AMBER force field was utilized in this work.[5, 6] While a cut-off distance of 12 Å was used for the Lennard-Jones potential, the long-ranged interactions were accounted for by calculating tail correction approximation and particle-particle particle-mesh algorithm.[7] The RESP method was employed to calculate atomic partial charges [8]. Polarizability in ions was induced by scaling the partial charges by a factor of 0.74 that showed only 2% difference from experimental values in ambient conditions.[9, 10] In order to optimize an isolated ion structure, Gaussian 09 software was used to perform the calculation on B3LYP/6-311++g(d,p) level.[11] The temperature and pressure were held constant by utilizing the Nosé–Hoover thermostat and barostat, respectively.[12, 13] The periodic boundary condition was applied in all three directions. The size of the system was 49680 atoms that bringing it to a total number of 1080 ion pairs within the simulation box. All the calculations of the system properties were performed based on five replicas to increase the statistical accuracy of obtained results. All of the simulations were performed in LAMMPS package.[14]

The mean squared displacement was calculated using coordinates of the center of mass of the anions and cations over 10 ns in *NVT* ensemble simulation. The temperatures ranging from 240 K (glassy state) to 640 K (liquid state) were analyzed to access the full evolution of the dynamics in the system. The relaxation times obtained from TTS and ISF calculations for ILs were obtained by following the same procedure that is described in the main text of the manuscript for the model thermoset and vitrimer. The reader is referred to our previous work for a complete description of calculations and results of the ionic liquid system.[9]

References

1. Mason, T. G.; Weitz, D. A. Optical Measurements of Frequency-Dependent Linear Viscoelastic Moduli of Complex Fluids. *Physical review letters* **1995,** 74 (7), 1250.
2. Furst, E. M.; Squires, T. M., *Microrheology*. Oxford University Press: 2017.
3. Li, Q.; Peng, X.; Chen, D.; McKenna, G. B. The Laplace Approach in Microrheology. *Soft Matter* **2020,** 16 (14), 3378-3383.
4. Mason, T. G. Estimating the Viscoelastic Moduli of Complex Fluids Using the Generalized Stokes-Einstein Equation. *Rheol. Acta* **2000,** 39 (4), 371-378.
5. Wang, J.; Wang, W.; Kollman, P. A.; Case, D. A. Automatic Atom Type and Bond Type Perception in Molecular Mechanical Calculations. *J Mol Graph Model* **2006,** 25 (2), 247-60.
6. Wang, J.; Wolf, R. M.; Caldwell, J. W.; Kollman, P. A.; Case, D. A. Development and Testing of a General Amber Force Field. *J. Comput. Chem.* **2004,** 25 (9), 1157-1174.
7. Hockney, R. W.; Eastwood, J. W., *Computer Simulation Using Particles*. crc Press: 1988.
8. Bayly, C. I.; Cieplak, P.; Cornell, W.; Kollman, P. A. A Well-Behaved Electrostatic Potential Based Method Using Charge Restraints for Deriving Atomic Charges: The Resp Model. *J. Phys. Chem.* **1993,** 97 (40), 10269-10280.
9. Balogun, A.; Lazarenko, D.; Khabaz, F.; Khare, R. Extending the Timescale of Molecular Simulations by Using Time–Temperature Superposition: Rheology of Ionic Liquids. *Soft Matter* **2021,** 17 (30), 7210-7220.
10. Zhang, Y.; Maginn, E. J. A Simple Aimd Approach to Derive Atomic Charges for Condensed Phase Simulation of Ionic Liquids. *J. Phys. Chem. B* **2012,** 116 (33), 10036-10048.
11. Frisch, M.; Trucks, G.; Schlegel, H. B.; Scuseria, G. E.; Robb, M. A.; Cheeseman, J. R.; Scalmani, G.; Barone, V.; Mennucci, B.; Petersson, G., Gaussian 09, Revision D. 01. Gaussian, Inc., Wallingford CT: 2009.
12. Hoover, W. G. Canonical Dynamics: Equilibrium Phase-Space Distributions. *Phys. Rev. A* **1985,** 31 (3), 1695.
13. Parrinello, M.; Rahman, A. Polymorphic Transitions in Single Crystals: A New Molecular Dynamics Method. *J. Appl. Phys.* **1981,** 52 (12), 7182-7190.
14. Plimpton, S. Fast Parallel Algorithms for Short-Range Molecular Dynamics. *J Comput Phys* **1995,** 117, 1-19.